Département de

GENIE MECANIQUE

جامعة باتنة 2

UB

UNIVERSITY OF BATNA 2

CERTIFICATE

OF PARTICIPATION

NCME'25

THE SECOND NATIONAL CONFERENCE ON ENGINEERING

This certificate is proudly presented to

ASSAS Taqiyeddine

who has participated in The Second National Conference On Mechanical Engineering NCME'25 on November 26th, 2025 at Mechanical Engineering Department, Mostefa BENBOULAID Batna 2 University.

Paper title : Mechanical and Thermal Buckling of FGM Plates Based on a Simple High-Order Shear Deformation Theory and Strain Based approach.

Co-authored by : CHENAFI Madjda , BOUREZANE Messaoud , BENABID Seyfeddine

Chairman of NCME'25
Dr Rafik MAKHLOUFI

The Second National Conference on Mechanical Engineering
University Batna 2
NCME'25
Mechanical Engineering Departement

Scientific Committee Chairman of NCME'25
Dr Mohamed MASMOUDI

The Second National Conference On Mechanical Engineering NCME'25

Département de
GENIE MECANIQUE

Batna, November 26th, 2025

The Second National Conference On Mechanical Engineering NCME'25

Département de GENIE MECANIQUE

Batna, November 26th, 2025

Conference Program

Time	Event
From 08h00	Welcome + Registration
09h00 - 09h30	Opening Ceremony
09h30 - 10h15	Plenary Session Pr. GUEZOULI Larbi " The Augmented Mechanical Engineer : Building Smarter with AI "
10h15 - 10h45	Tribute to Prof. SI AMEUR Mohamed
	Retirement Recognition Ceremony
10h45- 11h00	Coffee Break
11h00 - 12h00	Poster Session 1
12h00 - 13h30	Lunch
13h30 - 14h30	Oral Session
14h30 - 14h45	Coffee Break
14h45 - 15h45	Poster Session 2
16h00	Certificate Awarding + Closing Ceremony

The Second National Conference On Mechanical Engineering NCME'25

Département de GENIE MECANIQUE

Batna, November 26th, 2025

Poster Session 1

11h00 - 12h00

Researcher	Title	Code
BECHIRI Sarra	3D Finite Element Modeling and Analysis of Femur Bone with ANSYS Workbench.	CM01
BENBOUTA Soumia	Static study and identification of operational limits of a Darrieus H wind turbine rotor.	CM02
CHICHOUNE Samira	A new strain based rectangular finite element with drilling rotation for static and dynamic analysis.	CM03
ZITOUNI Hadda	Study of load transfer (dive) during braking with ABS.	CM04
YOUSFI Hichem	Developing an Advanced Topology Optimization Methodology for Industrial Components Using Digital Simulation Techniques.	CM05
RHASKALI Boulenouar	Mis en évidence de la charge dangereuse responsable des lésions du ligament croisé antérieur (LCA).	CM06
SAHNOUN Abdelfettah	Investigating Follower-Force Effects on Shear-Deformable Beam Deflection via Finite Elements.	CM07
ARAR Karim	Biomechanical Modelling and Simulation of Musculoskeletal Assistance in the Human Hip Joint.	CM08
KARECHE Abdelhak	Contribution of date-palm fibers reinforcement to cement mortar performances	ECPM 01
KHELIFI Halima	Improving the Fatigue Resistance of X70 Steel through Boriding Process.	ECPM 02
DAAS Ahmed	Enhancing the Fatigue Resistance of API X70 Steel through Microstructural Control.	ECPM 03
BRIKI Lyamine	Valorization of granite waste in the formulation of mortars.	ECPM 04
NACER Sarra	Effect of complex fiber shape on effective elastic moduli of composites.	ECPM 05
BOULTIF Amira	Investigation of Interface and Interphase Effects on the Elastic Behavior of Fiber Reinforced Composite (FRC).	ECPM 06
KENISSE Noussaiba	Numerical Evaluation of Effective Thermal Properties in Composites: Direct vs. Multi-Step Homogenization.	ECPM 07

The Second National Conference On Mechanical Engineering NCME'25

Département de GENIE MECANIQUE

Batna, November 26th, 2025

BAROURA Lazhar1	Study of the Influence of Resistance Spot Welding Parameters on the Thermal and Mechanical Behavior of Metallic Assemblies	ECPM 08
TADEGHT Mohammed	Effects of Grain Size and Grinding Parameters on Surface Finish and Forces in Grinding	MM01
SACI Rebai	Machining by electro-erosion (EDM) for hard materials.	MM02
ZAHAF Mohamed Zakaria	Multi-objective optimization of end milling parameters for surface roughness in as-received and hardened bearing Steel	MM03
AFIF Fouad	Fraisage du Z200C12: Optimisation multi-objectif des paramètres de coupe par ANOVA et fonction de désirabilité.	MM04
BOUTAGHANE Ayoub	CFD-Driven Structural and Operational Geometry Enhancements in PEM Electrolyzers for Improving Mass Transport.	TF 01
HADDAD Zakaria	Effect of Surface Geometry on Flow Stability.	TF 02
LAMNIAI Choukry	Simulation of heat transfert between a heat source and PCM in a 2D cylindrical model on Matlab.	TF 03
SAFA Safia	Effect of nanofluid variable properties on natural convection in annular enclosure under inclined magnetic field.	TF 04
ACHI Alladdine	Validation of the new library called Baffle3DRegion in Open FOAM.	TF 05
CHAOUI Assil	Thermo-Hydraulic Performance Enhancement of Shell and Tube Heat Exchangers Using Novel Internal Geometries.	TF 06
ZEMMOURI Fayza	Calculation of VLE Data for Ternary Refrigerant Mixtures by PC-SAFT Equation of State.	TF 07
AMIAR Ali	Étude de l'impact des facteurs environnementaux sur les performances des panneaux solaires photovoltaïques dans la région d'Ouargla.	TF 08
MCHOUNCHI Lahcen	Comparison of the Performance of R600a, R1234yf, R290 and R1234ze Refrigerants in an Ejector Refrigeration Cycle.	TF 09
MEZAACHE Abderrahmane	Heat transfer and entropy generation in a convergent-divergent channel heat exchanger.	TF 10
BENAOUA Salah	Lattice Boltzmann simulation of mixed convection in a bottom heated vented square cavity.	TF 11

The Second National Conference On Mechanical Engineering NCME'25

Département de GENIE MECANIQUE

Batna, November 26th, 2025

Oral Session 13h30 - 14h30	
Researcher	**Title**
ASSAS Taqiyeddine	Mechanical and Thermal Buckling of FGM Plates Based on a Simple High-Order Shear Deformation Theory and Strain Based approach.
GHODBANE Hassina	Modeling and Simulation of Combustion Dynamics and Performance in Hydrogen-Fueled Engines.
SELLOUM Rabia	Post-quantum protocols for CAD/CAM data protection

Poster Session 2 14h45 - 15h45		
Researcher	**Title**	**Code**
LARIBI Anfel	Examination of stress distributions in thick-walled composite pipes subjected to bending forces.	CM09
MASMOUDI Mohamed	Single Over Head Camshaft versus Free Valve system of the automotive Engine. Numerical Simulations.	CM10
KAAROUCHE Rayene	Design and Implementation of a Low-Cost Portable Negative Pressure Wound Therapy (NPWT).	CM11
MAACHE Abdelhak	De la biomécanique - la prothèse : l'évolution des implants totaux du genou.	CM12
ACHOURI Samir	Effect of Diaphyseal Plate Thickness on the Initial Damage Cycle.	CM13
BENNACEUR Hamza	Methodology for the Generation of Quasi-Isotropic and Graded Lattice Structures within Complex Design Environments.	CM14

The Second National Conference On Mechanical Engineering NCME'25

Département de GENIE MECANIQUE

Batna, November 26th, 2025

BOUANAKA Mohamed Larbi	A Novel membrane finite element based on the strain approach for elastic and elastoplastic analysis.	CM15
ASSAS Taqiyeddine	Mechanical Buckling of FGM Plates Based on a Simple High-Order Shear Deformation Theory and Strain Based approach.	CM16
HAMADI Latifa	Electrochemical study of l-arginine as a corrosion inhibitor for a50 steel in hydrochloric acid.	ECPM 09
LAOUAR Abdelhamid	Numerical study of the effect of inclusion size on the effective electrical conductivity of composite materials.	ECPM 10
DJEBARA Youcef	3D Spherulite Modelling and Elastic Property Evaluation of Semi-Crystalline Polymers.	ECPM 11
BOUSSAHA Ahmed	Identification and Characterization of a Steel Located at the Technology Hall of Batna 2 University.	ECPM 12
TOULMIT Noureddine	Integration of SOLIS-H_2 System for Hydrogen Production via Thermal Recovery at the Ain Djasser Gas Power Plant (Algeria).	ECPM 13
BAALI Khouloud	Study of metallurgical properties in fluxes with Submerged arc welding.	ECPM 14
BAROURA Lazhar	Grey Relational Optimization of Grinding Parameters for Gas-Carburized Low-Carbon Steel	ECPM 15
BAITI Adel	Influence and Optimization of TiC Addition on the Microstructural and Mechanical Behavior of NbC–Co Cermets Fabricated by Powder Metallurgy	ECPM 16
MEDEGHAGHET_Yassina	High-Efficiency Sensorless Field-Oriented Control of Induction Motors Using an Extended Kalman Filter Considering core Loss.	ECPM 17
ABDESSEMED Abdelhakim	Residual Stress Mitigation in Additively Manufactured Turbine Blades.	MM05
SELLOUM Rabia	High-Fidelity Alignment of Helical Gear Models Using Synthetic Point Clouds, GAN-Based Reconstruction, and Enhanced ICP.	MM07
MEKENTICHI Sif-Eddine	Influence of radial depth of cut on cutting forces in ball end milling using a mechanistic approach.	MM08

The Second National Conference On Mechanical Engineering NCME'25

Département de GENIE MECANIQUE

Batna, November 26th, 2025

MOHAMMED CHERIF Okba	Thermal Design for Selecting Silicon Carbide MOSFETs in Power Converters.	TF 12
BOUKHAMLA Halima	Enhancing Solar Chimney Power Plant Performance through a Modified Collector and Radial Inflow Turbine: A CFD Analysis.	TF 13
LACHRAF Abdelbasset	Flow, combustion and thermal characteristics of hydrogen fueled microcombustor with trapezoidal ribs: effect of ribs number.	TF 14
FERRAK Intissar	Validation of Sorption Isotherm Models: Insights into Hysteresis and Hygrothermal Behavior of Perforated Bricks.	TF 15
CHABANI Ines	Performance improvement of a solar thermal storage system using nano-enhanced phase change materials.	TF 16
GUERBAZI Mohamed El Amine	Integrated Simulation of High-Temperature PEM Fuel Cell and Absorption Cooling System for Enhanced Energy Efficiency.	TF 17
MERIMECHE Imene	Heat Transfer Enhancement in absorber tubes by combining vortex generators with nanofluids.	TF 18
SIDIALI Amira	Comparative Analysis of Fin Geometries for Enhanced Direct Steam Generation in Parabolic Trough Collectors.	TF 19
MEDERHARHET Yassina	High-Efficiency Sensorless Field-Oriented Control of Induction Motors Using an Extended Kalman Filter Considering core Loss.	TF 21
BENABID Farida	Influence of Slot Conductor Spacing and Copper Losses on Winding Hot-Spot Temperature: Heat Transfer Analysis.	TF 22
BOUKARANA Leila	Power System Control Using a Unified Power Flow Controller (UPFC).	TF 23
BOUZID Aissa	Analysis of Sealed Medium Motion in Labyrinth Seals: Frequency and Amplitude Effects with Chamber-Resolved Flow Properties	ON Line
Bensaadia Amira	Static and forced vibration analysis of membrane structures by strain based formulation	MM09

The Second National Conference on Mechanical Engineering
NCME'25
Batna 2 Mostefa BENBOULAID University
November 26, 2025

Research Paper

Mechanical Buckling of FGM Plates Based on a Simple High-Order Shear Deformation Theory and Strain Based approach

ASSAS Taqiyeddine [a,*], CHENAFI Madjda [a], BOUREZANE Messaoud [a], BENABID Seyfeddine [b]

[a] *Laboratory of Hydraulic Developments and Environment (LAHE), Civil Engineering and Hydraulic Department, University of Biskra, Biskra, Algeria*

[b] *Research Laboratory in Subterranean and Surface Hydraulics, LARHYSS, Civil Engineering and Hydraulic Department, University of Biskra, Biskra, Algeria*

ARTICLE INFO

Article history:

Received 00 January20

Received in revised form 00 February20

Accepted 00 February 20

Keywords:

Buckling behavior; Functionally graded; High-order shear deformation theory ; Strain-based approach

ABSTRACT

The buckling behavior of functionally graded rectangular plates subjected to mechanical loads is analyzed using a four-node finite element formulated within the framework of a refined high-order shear deformation theory and strain-based approach. Unlike traditional higher-order models, the proposed formulation reduces the number of independent variables to five by enforcing zero transverse shear stress conditions on the top and bottom surfaces and adopting a quadratic distribution of transverse shear strains through the plate thickness. This model inherently satisfies the traction-free boundary conditions on the outer surfaces of the plate, eliminating the need for shear correction factors. Each node of the element includes five degrees of freedom, achieved by combining a two-degree-of-freedom membrane element with a three-degree-of-freedom bending plate element. The finite element formulation is derived from the principle of total potential energy, leading to the development of both stiffness and geometric matrices. Additionally, the position of the neutral surface is determined, and the corresponding buckling stability equations are formulated with respect to this reference surface. Convergence and comparative studies confirm the robustness and accuracy of the developed element in predicting the critical buckling loads thresholds for both isotropic and functionally graded material (FGM) plates. Parametric investigations are conducted to examine the influence of the volume fraction exponent, aspect ratio, and loading conditions on the overall buckling behavior of FG plates.

1 Introduction

Functionally graded materials (FGMs) have attracted considerable interest in recent years due to their ability to seamlessly integrate the advantageous properties of two or more constituent materials—typically a ceramic and a metal. These materials feature a continuous variation in composition and material properties through their thickness, which effectively mitigates issues such as delamination and stress concentrations commonly observed in traditional laminated composites [1], [2].

* *Corresponding author. Tel.: 0670-87-61-31.*
E-mail address: taqiyeddine.assas@univ-biskra.dz

As a result, FGMs are highly suitable for applications that require both thermal resistance and structural integrity, such as those in the aerospace, nuclear, and biomedical engineering fields [3], [4]. Among various structural components made from FGMs, thin plates are extensively used in engineering structures. The stability of these plates under different loading conditions is critical to ensuring structural performance and safety. Buckling, one of the most common failure modes in plate structures, has been widely studied in this context. Classical plate theory (CPT) and first-order shear deformation theory (FSDT) are commonly applied in such analyses; however, they fail to accurately capture transverse shear deformation, particularly in thick plates [5]. Higher-order shear deformation theories (HSDTs), by contrast, provide improved accuracy by incorporating a more realistic representation of the transverse shear strain distribution through the plate thickness [6], [7]. Despite their advantages, conventional HSDTs often involve a greater number of unknowns and require shear correction factors to satisfy traction-free boundary conditions, thereby increasing the complexity and computational cost of the models [8]. To overcome these challenges, strain-based formulations have emerged as efficient alternatives. These approaches reduce the number of unknowns while inherently satisfying the zero transverse shear stress conditions at the top and bottom surfaces of the plate [9].

In the present study, a novel finite element model is developed to analyze the buckling behavior of functionally graded quadrilateral plates subjected to mechanical loads. The model is based on a simplified higher-order shear deformation theory combined with a strain-based finite element formulation. It assumes a quadratic variation of transverse shear strains through the thickness, enabling the enforcement of traction-free conditions without requiring shear correction factors. The proposed four-node element incorporates five essential degrees of freedom per node by superimposing a membrane element (with two degrees of freedom per node) [10] and a bending plate element (with three degrees of freedom per node) [11]. The formulation is derived using the principle of total potential energy, and the position of the neutral surface is determined to enhance the accuracy of the stability analysis. The finite element model is implemented using an in-house MATLAB code and validated through convergence studies and comparison with existing results from the literature. The study also explores the influence of several key parameters—including the volume fraction exponent, side-to-thickness ratio, aspect ratio, and loading conditions—on the critical buckling behavior of functionally graded plates. The findings confirm the accuracy and efficiency of the proposed method in predicting buckling responses for both isotropic and functionally graded material plates.

2 Materials and Methods

2.1 Functionally Graded Materials

Functionally graded materials (FGMs) are advanced composite materials characterized by a continuous variation of material properties across their thickness. Typically, FGMs are composed of two or more constituent materials, such as ceramics and metals, whose volume fractions vary gradually to achieve desired performance characteristics , as illustrated in Figure 1. This gradation helps to eliminate abrupt interfaces found in traditional laminated composites, reducing the risk of delamination and stress concentrations.

In this study, the FGM plate consists of a ceramic phase and a metallic phase. The material properties vary continuously in the thickness direction according to a power-law distribution based on the volume fraction of the constituents. The volume fraction of the ceramic phase at any thickness coordinate z is expressed as [12]:

$$V_c(z) = \left(\frac{z}{h} + \frac{1}{2}\right)^p \quad (1)$$

$$P(z) = P_m + (P_c - P_m)\, V_c(z) \quad (2)$$

where h is the total thickness of the plate, z is the coordinate measured from the mid-plane (ranging from −h/2 to h/2), and p is the volume fraction exponent that governs the gradation profile and the indicators m and c describe the metal and ceramic, respectively, P_c and P_m are the corresponding material characteristics, such as density (ρ), Young's modulus (E), and other characteristics. (p≥0) represents the gradient index of martial FGM

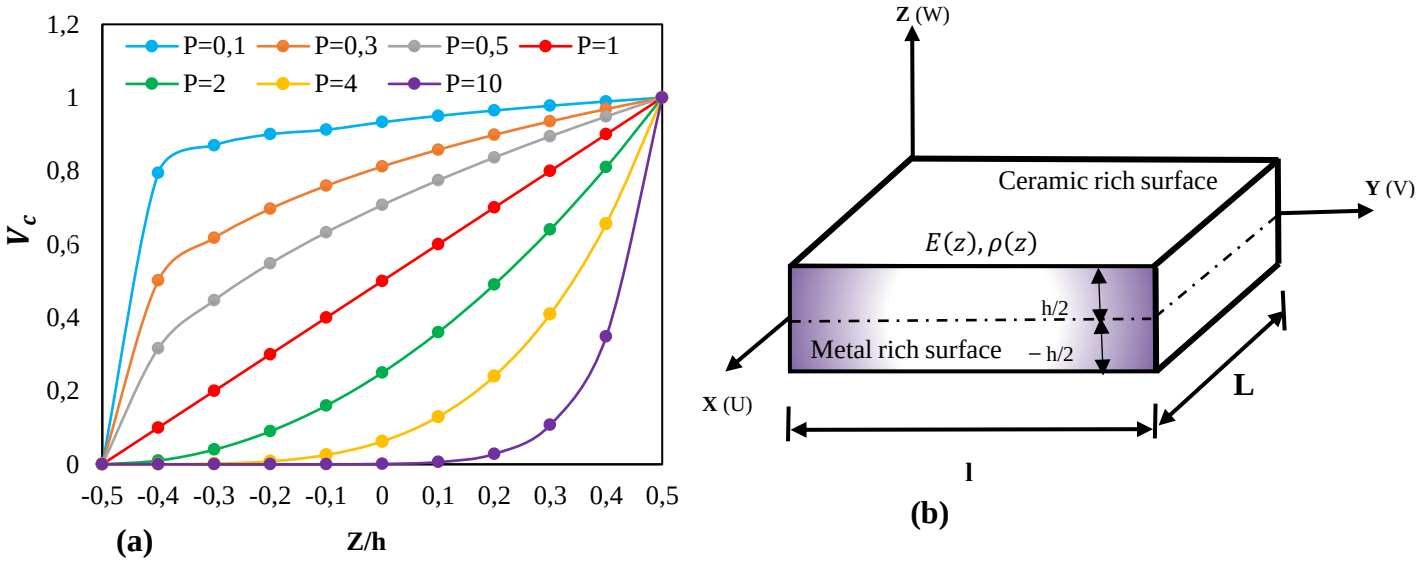

Fig. 1 (a) Variation of the ceramic volume fraction Vc(z) across the plate thickness for different values of power-law index p. **(b)** Geometry and coordinate system of the functionally graded plate

2.2 Displacement field and cinematics

According to Figure 1.b and following the simple high-order shear deformation theory (HSDT) proposed by Tati [9], the displacement components $u(x,y,z)$;$v(x,y,z)$, and $w(x,y,z)$ at a point in the plate are expressed as.:

$$\begin{aligned} u(x,y,z) &= u_0(x,y,z) + z\phi_x(x,y) \\ v(x,y,z) &= v_0(x,y,z) + z\phi_y(x,y) \\ w(x,y,z) &= f(z)w_0(x,y) + (f(z)-1)G(x,y) \end{aligned} \tag{3}$$

Where $G(x,y)$ is a function defiend by:

$$\phi_x(x,y) = \frac{\partial G(x,y)}{\partial x} \quad \phi_y(x,y) = \frac{\partial G(x,y)}{\partial y} \tag{4}$$

- $u_0(x,y,z)$, $v_0(x,y,z)$, $w_0(x,y)$: are the mid-plane displacements in the x, y, z directions, respectively.
- $\phi_x(x,y)$, $\phi_y(x,y)$: are rotations of the normal to the mid-surface due to bending.
- $f(z) = \frac{5}{4}\left(1 - \frac{4z^2}{h^2}\right)$: is a shape function representing the parabolic distribution of transverse shear strains through the thickness, often chosen to satisfy zero shear stress on the top and bottom surfaces.

Based on the displacement field defined in Section 2.2, the normal and in-plane shear strains in the plate can be expressed in matrix form as [13]:

$$\{\varepsilon\} = \begin{Bmatrix} \varepsilon_x \\ \varepsilon_y \\ \gamma_{xy} \end{Bmatrix} = \{\varepsilon^0\} + z\{\kappa\} = \begin{Bmatrix} \varepsilon_x^0 \\ \varepsilon_y^0 \\ \gamma_{xy}^0 \end{Bmatrix} + z\begin{Bmatrix} \kappa_x \\ \kappa_y \\ \kappa_{xy} \end{Bmatrix} \tag{5}$$

$$\{\gamma_z\} = \begin{Bmatrix} \gamma_{xz} \\ \gamma_{yz} \end{Bmatrix} = f(z)\begin{Bmatrix} \gamma_{xz}^0 \\ \gamma_{yz}^0 \end{Bmatrix} \tag{6}$$

2.3 Constitutive relations

The constitutive equations of an elastic FGM plate can be given by

$$\begin{Bmatrix} \sigma_{xx} \\ \sigma_{yy} \\ \tau_{xy} \end{Bmatrix} = \begin{bmatrix} C_{11} & C_{12} & 0 \\ C_{21} & C_{22} & 0 \\ 0 & 0 & C_{66} \end{bmatrix} \begin{Bmatrix} \varepsilon_{xx} \\ \varepsilon_{yy} \\ \gamma_{xy} \end{Bmatrix} \tag{7}$$

Or

$$\{\sigma\} = [C]\{\varepsilon\} \tag{8}$$

$$\begin{Bmatrix}\tau_{xz}\\ \tau_{yz}\end{Bmatrix}=\begin{bmatrix}C_{44} & 0\\ 0 & C_{55}\end{bmatrix}\begin{Bmatrix}\gamma_{xz}\\ \gamma_{yz}\end{Bmatrix} \quad (9)$$

Where $(\sigma_{xx},\ \sigma_{yy},\ \tau_{xy},\ \tau_{xz},\ \tau_{yz})$ and $(\varepsilon_{xx},\ \varepsilon_{xx},\ \gamma_{xy},\ \gamma_{xz},\ \gamma_{yz})$ are the stresses and strains, respectively.The rigidity coefficients C_{ij} can be formulated according to the material properties given in Eq.2 as follows:

$$C_{11}(z)=C_{22}(z)=\frac{E(z)}{1-\nu^2}\ ;\ C_{12}(z)=C_{21}(z)=\nu\frac{E(z)}{1-\nu^2};$$
$$C_{44}(z)=C_{55}(z)=C_{66}(z)=\frac{E(z)}{2(1+\nu)} \quad (10)$$

2.4 The force and moment resultants

In functionally graded plates, due to the asymmetry in material distribution through the thickness, the physical neutral plane does not coincide with the geometric mid-plane. This asymmetry leads to membrane-bending coupling, which must be avoided for accurate analysis.To decouple membrane and bending behavior, all force and moment resultants are calculated with respect to the physical neutral surface, as illustrated in Figure 2[14].

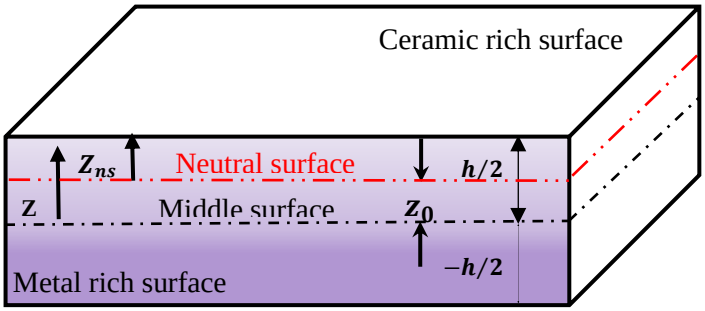

Fig. 2 Position of the neutral plane of FGM plate

The position z_0 of the neutral surface (measured from the mid-plane) is defined such that the bending-extensional coupling terms vanish:

$$\int_{-\frac{h}{2}}^{\frac{h}{2}}\big(E(z)(z-z_0)\big)dz=0,\ \int_{-\frac{h}{2}}^{\frac{h}{2}}E(z)zdz-(z_0)\int_{-\frac{h}{2}}^{\frac{h}{2}}E(z)dz=0 \quad (11)$$

The position of the physical neutral plane is given by [15]

$$z_0=\frac{\int_{-\frac{h}{2}}^{\frac{h}{2}}\mathrm{E(z)zdz}}{\int_{-\frac{h}{2}}^{\frac{h}{2}}\mathrm{E(z)dz}} \quad (12)$$

The **membrane forces**, **bending moments**, and **transverse shear forces** per unit length in a functionally graded plate are obtained by integrating the stress components through the plate thickness, relative to the neutral surface at $z=z_0$

$$\begin{Bmatrix}N_x\\ N_y\\ N_{xy}\end{Bmatrix}=\int_{-\frac{h}{2}}^{\frac{h}{2}}\begin{Bmatrix}\sigma_x(z)\\ \sigma_y(z)\\ \tau_{xy}(z)\end{Bmatrix}\mathrm{dz} \quad (13.a)$$

$$\begin{Bmatrix}M_x\\ M_y\\ M_{xy}\end{Bmatrix}=\int_{-\frac{h}{2}}^{\frac{h}{2}}\begin{Bmatrix}\sigma_x(z)\\ \sigma_y(z)\\ \tau_{xy}(z)\end{Bmatrix}(\mathrm{z}-z_0)\ \mathrm{dz} \quad (13.b)$$

$$\begin{Bmatrix}T_x\\ T_y\end{Bmatrix}=\int_{-\frac{h}{2}}^{\frac{h}{2}}\begin{Bmatrix}\tau_{xz}\\ \tau_{yz}\end{Bmatrix}\mathrm{dz} \quad (13.c)$$

The relationship between the **stress resultants** (membrane forces {N} bending moments {M}, and transverse shear forces {T}and the corresponding **generalized strains** (membrane strains ε^m, curvatures κ, and shear strains γ) is given by:

$$\begin{Bmatrix}N\\ M\\ T\end{Bmatrix}=\begin{bmatrix}[A] & 0 & 0\\ 0 & [\mathrm{B}] & 0\\ 0 & 0 & [\mathrm{S}]\end{bmatrix}\begin{Bmatrix}\varepsilon^m\\ \kappa\\ \gamma\end{Bmatrix} \quad (14)$$

where the constitutive matrices for membrane $[A]$, bending [B], and shear [S] are defined according to the formulations provided by Sedgui et al. [16]:

$$[A] = \begin{bmatrix} 1 & \nu & 0 \\ \nu & 1 & 0 \\ 0 & 0 & \frac{1-\nu}{2} \end{bmatrix} \int_{-h/2}^{h/2} \frac{E(z)}{(1-\nu^2)} dz \tag{15}$$

$$[B] = \begin{bmatrix} 1 & \nu & 0 \\ \nu & 1 & 0 \\ 0 & 0 & \frac{1-\nu}{2} \end{bmatrix} \int_{-h/2}^{h/2} \frac{E(z)}{(1-\nu^2)} (z - z_0)^2 dz \tag{16}$$

$$[S] = \begin{bmatrix} 1 & 0 \\ 0 & 1 \end{bmatrix} \int_{-h/2}^{h/2} \frac{E(z)}{2(1+\nu)} (f(z))^2 dz \tag{17}$$

3 Finite Element Formulation of the Proposed RSBP20 Element

The proposed RSBP20 (Rectangular Strain Based Plate) finite element is a four-node Rectangular plate element designed for the buckling analysis of functionally graded material (FGM) plates. Each node includes five degrees of Freedom : {u,v,w, φ_x, φ_y} as shown in Figure 3.

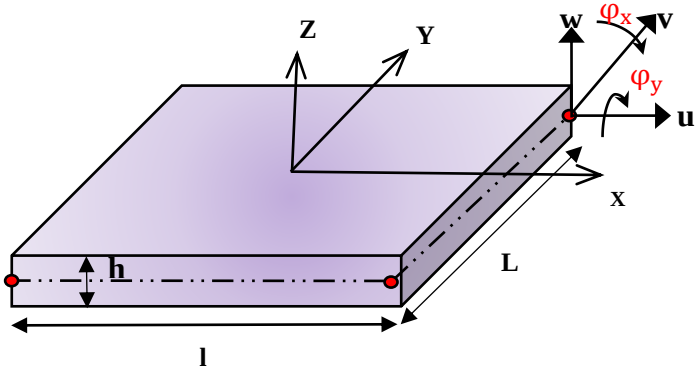

Fig. 3 Geometry and nodal variables of the finite element

The displacement field of the element is constructed by the **superposition** of two independent strain-based elements:

- ✓ **Membrane Element** (Sabir and Sfendji [10])

$$\{U_m\} = \begin{Bmatrix} u \\ v \end{Bmatrix} = [P_m]\{\alpha_m\} \tag{18}$$

Where $\{\alpha_m\}^T = \{\alpha_1, \ldots \alpha_8\}$

$$[P_m] = \begin{bmatrix} 1 & 0 & -y & x & xy & 0 & -\frac{y^2}{2} & \frac{y}{2} \\ 0 & 1 & x & 0 & -\frac{x^2}{2} & y & xy & \frac{x}{2} \end{bmatrix} \tag{19}$$

- ✓ **Reissner–Mindlin Plate Element (Belounar et al. [33])**

The displacement functions for bending plate element (SBRP) are [11]:

$$\{U_b\} = \begin{Bmatrix} w \\ \beta_x \\ \beta_y \end{Bmatrix} = [P_b]\{\alpha_b\} \tag{20}$$

Where $\{\alpha_b\}^T = \{\alpha_9, \ldots \alpha_{20}\}$

$$[P_b] = \begin{bmatrix} 1 & -x & -y & -\frac{x^2}{2} & -\frac{x^2 y}{2} & -\frac{y^2}{2} & -\frac{xy^2}{2} & -\frac{xy}{2} & \frac{x}{2} & \frac{xy}{2} & \frac{y}{2} & \frac{xy}{2} \\ 0 & 1 & 0 & x & xy & 0 & -\frac{y^2}{2} & \frac{y}{2} & \frac{1}{2} & \frac{y}{2} & 0 & -\frac{y}{2} \\ 0 & 0 & 1 & 0 & -\frac{x^2}{2} & y & xy & \frac{x}{2} & 0 & -\frac{x}{2} & \frac{1}{2} & \frac{x}{2} \end{bmatrix} \tag{21}$$

Thus, the **RSBP20 element** includes a total of **20 degrees of freedom**, with its full displacement field expressed as :

$$\{U_e\}=\begin{Bmatrix} u \\ v \\ \theta_z \\ w \\ \varphi_x \\ \varphi_y \end{Bmatrix}=\begin{bmatrix}[P_m] & 0 \\ 0 & [P_b]\end{bmatrix}\begin{Bmatrix}\{\alpha_m\} \\ \{\alpha_b\}\end{Bmatrix}=[P]\{\alpha\}$$

Where $\{\alpha\}^T=\{\{\alpha_m\}\,\{\alpha_b\}\}^T=\{\alpha_1,\dots\alpha_{20}\}^T$

$$[P]=\begin{bmatrix}[P_m] & [0] \\ [0] & [P_b]\end{bmatrix} \tag{36}$$

$$[P]=\left[\begin{array}{cccccccc|cccccccccccc}
1 & 0 & -y & x & xy & 0 & -\frac{y^2}{2} & \frac{y}{2} & 0 & 0 & 0 & 0 & 0 & 0 & 0 & 0 & 0 & 0 & 0 & 0 \\
0 & 1 & x & 0 & -\frac{x^2}{2} & y & xy & \frac{x}{2} & 0 & 0 & 0 & 0 & 0 & 0 & 0 & 0 & 0 & 0 & 0 & 0 \\
\hline
0 & 0 & 0 & 0 & 0 & 0 & 0 & 0 & 1 & -x & -y & -\frac{x^2}{2} & -\frac{x^2y}{2} & -\frac{y^2}{2} & -\frac{(xy)^2}{2} & -\frac{xy}{2} & \frac{x}{2} & \frac{xy}{2} & \frac{y}{2} & \frac{xy}{2} \\
0 & 0 & 0 & 0 & 0 & 0 & 0 & 0 & 0 & 1 & 0 & x & xy & 0 & -\frac{y^2}{2} & \frac{y}{2} & \frac{1}{2} & \frac{y}{2} & 0 & -\frac{y}{2} \\
0 & 0 & 0 & 0 & 0 & 0 & 0 & 0 & 0 & 0 & 1 & 0 & -\frac{x^2}{2} & y & xy & \frac{x}{2} & 0 & -\frac{x}{2} & \frac{1}{2} & \frac{x}{2}
\end{array}\right]$$

The transformation matrix [C], which relates the vector of elemental nodal displacements $\{\boldsymbol{\delta^e}\}^{\mathbf{T}}=\left\{\boldsymbol{u_i, v_i, w_i,\ \varphi_{x_i}, \varphi_{y_i}}\right\}_{\boldsymbol{i=1,2,3,4}}$ to the vector of constants $\{\boldsymbol{\alpha}\}$, can be expressed in matrix form as follows:

$$\{\delta^e\}=[C]\,\{\alpha\} \tag{37}$$

Where

$$[C]=\{[P_1(x_i,y_i)]\;[P_2(x_i,y_i)]\;[P_3(x_i,y_i)]\;[P_4(x_i,y_i)]\}^{\mathrm{T}} \tag{38}$$

And (x_i, y_i) are the coordinates of the four node i (i = 1, 2, 3, 4)

3.1 Determination of the Strain Matrices

The strains- displacements relationship is obtained by

$$\{\varepsilon_m\}=[Q_m][C]^{-1}\{q_e\}=[B_m]\{q_e\} \tag{39}$$

$$\{\kappa\}=[Q_b][C]^{-1}\{q_e\}=[B_b]\{q_e\} \tag{40}$$

$$\{\gamma\}=[Q_s][C]^{-1}\{q_e\}=[B_s]\{q_e\} \tag{41}$$

$$\{\varepsilon^g\}=[G][C]^{-1}\{q_e\}=[B_g]\{q_e\} \tag{42}$$

Where

$$[Q_m]=\begin{bmatrix}\frac{\partial}{\partial x} & 0 & 0 \\ 0 & \frac{\partial}{\partial y} & 0 \\ \frac{\partial}{\partial y} & \frac{\partial}{\partial x} & 0\end{bmatrix}\begin{Bmatrix}u \\ v\end{Bmatrix};\ [Q_b]=\begin{bmatrix}0 & \frac{\partial}{\partial x} & 0 \\ 0 & 0 & \frac{\partial}{\partial y} \\ 0 & \frac{\partial}{\partial y} & \frac{\partial}{\partial x}\end{bmatrix}\begin{bmatrix}w \\ \beta_x \\ \beta_y\end{bmatrix};\ [Q_s]=\begin{bmatrix}\frac{\partial}{\partial x} & 1 & 0 \\ \frac{\partial}{\partial y} & 0 & 1\end{bmatrix}\begin{bmatrix}w \\ \beta_x \\ \beta_y\end{bmatrix};\ [G]=\begin{Bmatrix}\frac{\partial w}{\partial x} \\ \frac{\partial w}{\partial y}\end{Bmatrix} \tag{43}$$

For buckling response, a variation form of the virtual work principle according to the conditions of the FSDT may be written respectively, as [14]:

$$\delta\{\delta^e\}^T\left(\int_\Omega [B_m]^T[D_m][B_m]\;d\Omega\right)\{\delta^e\}+\delta\{\delta^e\}^T\left(\int_\Omega [B_b]^T[D_b][B_b]\;d\Omega\right)\{\delta^e\}$$
$$+\delta\{\delta^e\}^T\left(\int_\Omega [B_s]^T[D_s][B_s]\;d\Omega\right)\{\delta^e\}+\delta\{\delta^e\}^T\left(\int_\Omega [B_g]^T[\bar{N}][B_g]\;d\Omega\right)\{\delta^e\}=0 \tag{44}$$

Where the elementary matrices are mass and geometry ($[K_e]$ and $[K^e{}_g]$) is defined by the following equations:

$$[K_e]=\int_{-b}^{b}\int_{-a}^{a}\left(\underbrace{[B_m]^T[D_m][B_m]}_{Membrane}+\underbrace{[B_b]^T[D_b][B_b]}_{Bending}+\underbrace{[B_s]^T[D_s][B_s]}_{Shear}\right)dxdy \tag{45}$$

$$[K^e{}_g]=\int_\Omega [B_g]^T[\bar{N}][B_g]\,d\Omega \tag{46}$$

In which, $[\bar{N}]$ is the in-plane stresses of the matrix given bellow

$$[\bar{N}] = \begin{bmatrix} N_x & N_{xy} \\ N_{xy} & N_y \end{bmatrix} \quad (47)$$

4 Results and discussion

In this section, the buckling behavior of functionally graded (FG) plates is examined using the proposed finite element formulation. The obtained results are compared with available analytical and numerical solutions to validate the accuracy of the method. To demonstrate the effectiveness and applicability of the present approach, several numerical examples are conducted for various types of FG plates. The material properties used in these examples — including Young's modulus, Poisson's ratio, and density — are provided in Table 1. The geometry and loading of plates are shown in Fig. 4.

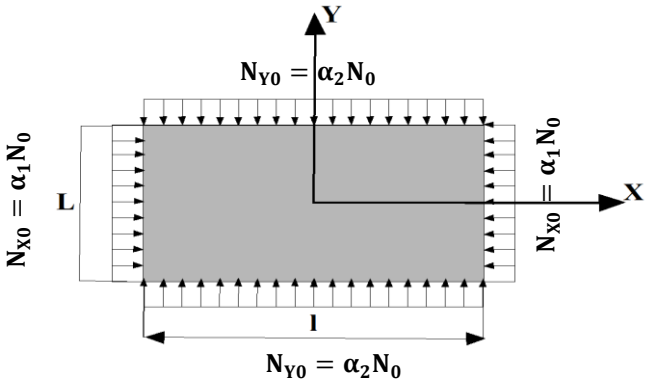

Fig. 4. Geometry and loading FGM rectangular plate.

Table 1 - Material parameters for the components of the FG plates

Properties	Metal		Ceramic		
	Aluminum* (Al*)	Aluminum (Al)	Zirconia ($ZrO_2 - 2$)	Aluinum ($ZrO_2 - 1$)	Aluminum (Al/Al_2O_3)
E(Gpa)	70	70	200	151	380
ν	0.3	0.3	0.3	0.3	0.3
ρ(kg/m^3)	2702	2707	5700	3000	3800

For simplicity, the critical buckling loads are presented in dimensionless form as follows:

$$\overline{\lambda_{cr}} = \lambda_{cr} \frac{(L^2)}{(E_m h^3)}. \quad (48)$$

The validity of the proposed element (RSBP20) is further assessed through the buckling analysis of simply supported (SSSS) Al/Al_2O_3 rectangular plates subjected to uniaxial (α1=1, α2=0) and biaxial (α1=1, α2=1) compressive loads, as illustrated in Figure 4. The plates are analyzed for aspect ratios l/L= =1 and 2, with a fixed slenderness ratio of l/h=100. The dimensionless critical buckling loads $\overline{\lambda_{cr}}$ of the functionally graded (FG) plates are presented in Tables 2 and 3, using five different values of the gradient index p.

This example is intended to examine the influence of the aspect ratio (l/L) and material gradient index (p) on the buckling behavior of FG plates. A comparison is made between the present results and those reported in the literature, including:

- The analytical solution of Reddy [17] based on Higher-Order Shear Deformation Theory (HSDT),
- The refined plate theory solution of Thai and Choi [18] using Levy's method,
- The refined HSDT results of Zenkour and Aljadani [19],
- The numerical results from Sadgui and Tati [16] using a Third-Order Shear Deformation Theory (TSDT), and
- The First-Order Shear Deformation Theory (FSDT) results of Belounar et al. [14].

The results obtained using the RSBP20 element show excellent agreement with those available in the literature, and in particular, they closely match the values reported by Reddy et al. [17].

From Tables 2–3 and Figure 5, it is evident that the dimensionless critical buckling load $\overline{\lambda_{cr}}$ under uniaxial loading is greater than that under biaxial loading. Additionally, for rectangular plates (l/L=2), the critical buckling loads are higher compared to square plates (l/L=1).

Figure 6 shows that the nondimensional critical buckling load under uniaxial compression increases with the length-to-thickness ratio l/h, indicating thinner FG plates have higher buckling resistance.

Figure 7 depicts the critical buckling load under biaxial compression rising with the length-to-width ratio l/L at l/h=100, showing that plates with higher aspect ratios exhibit greater buckling loads**.**

Table 2 - Nondimensionalized critical buckling ($\overline{\lambda_{cr}}$) of Al/Al_2O_3square plate (l/L = 1).

		gradient index p				
(α_1,α_2)	**Theory**	P =0	P =1	P =2	P =5	P =10
(1, 0)	**RSBP20 (20×20)**	**19.5702**	**9.7501**	**7.6160**	**6.4301**	**5.8604**
	Belounar et al. [14]	19.5534	9.7471	7.6058	6.4314	5.8576
	Sadgui and Tati [16]	19.6812	9.8107	7.6551	6.4724	5.8949
	Reddy [17]	**19.5700**	**9.7500**	**7.6100**	**6.4300**	**5.8600**
	Zenkour and Aljadani [19]	19.6145	9.7775	7.6293	6.4507	5.8752
	Thai and Choi [18]	19.6145	9.7775	7.6293	6.4507	5.8752
(1, 1)	**RSBP20 (20×20)**	**9.7880**	**4.8791**	**3.8066**	**3.2188**	**2.9320**
	Belounar et al. [14]	9.7767	4.8735	3.8029	3.2157	2.9288
	Sadgui and Tati [16]	9.8406	4.9053	3.8275	3.2362	2.9474
	Reddy [17]	**9.7880**	**4.8790**	**3.8070**	**3.2190**	**2.9320**
	Zenkour and Aljadani [19]	9.8072	4.8887	3.8146	3.2253	2.9375
	Thai and Choi [18]	9.8073	4.8888	3.8147	3.2254	2.9376

Table 3 - Nondimensionalized critical buckling ($\overline{\lambda_{cr}}$) of Al/Al_2O_3square plate (l/L = 2).

		gradient index p				
	Theory	P =0	P =1	P =2	P =5	P =10
(1, 0)	**RSBP20 (32×16)**	**77.7102**	**38.7404**	**30.2203**	**25.5405**	**23.2606**
	Belounar et al. [15]	78.0780	38.9208	30.3704	25.6808	23.3898
	Sadgui and Tati [13]	77.7471	39.2647	30.6328	25.8836	23.5667
	Reddy [17]	**77.7100**	**38.7400**	**30.2200**	**25.5400**	**23.2600**
	Zenkour and Aljadani [19]	78.3256	39.0545	30.4707	25.7491	23.4455
	Thai and Choi [18]	78.3257	39.0546	30.4707	25.7491	23.4456
(1,1)	**RSBP20 (32×16)**	**24.3782**	**12.5822**	**9.4822**	**8.0152**	**7.3001**
	Belounar et al. [15]	24.5111	12.2180	9.5339	8.0621	7.3430
	Sadgui and Tati [13]	24.6209	12.2748	9.5770	8.0948	7.3714
	Reddy [17]	**24.3780**	**12.5820**	**9.482**	**8.0150**	**7.299**
	Zenkour and Aljadani [19]	24.4974	12.2132	9.5293	8.0549	7.3353
	Thai and Choi [18]	24.4974	12.2132	9.5294	8.0550	7.3353

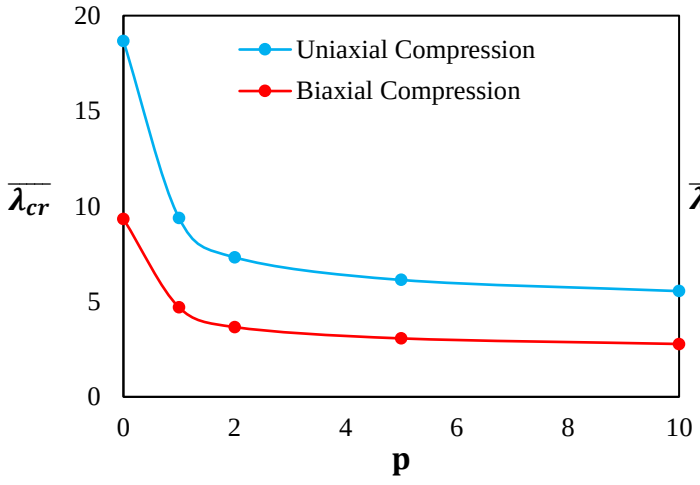

Fig.5. Impact of the in-plane loading on the nondimensionalized buckling load ($\overline{\lambda_{cr}}$) for a SSSS FG plate with different gradient index (p).

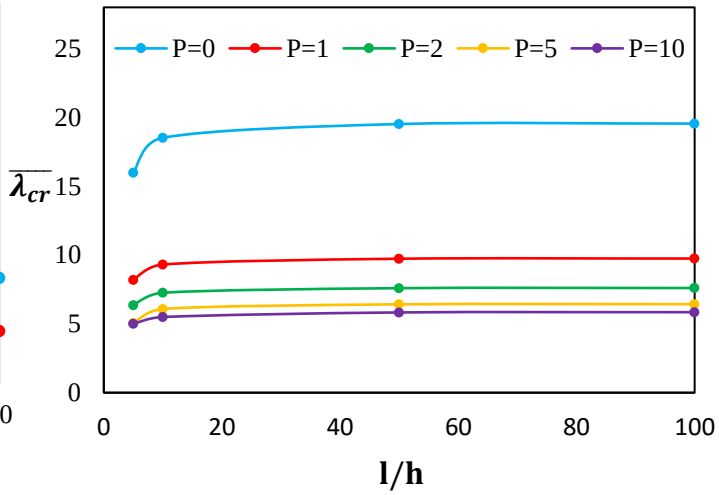

Fig.6. Nondimensionalized critical load factor ($\overline{\lambda_{cr}}$) of square plates versus side/ thickness

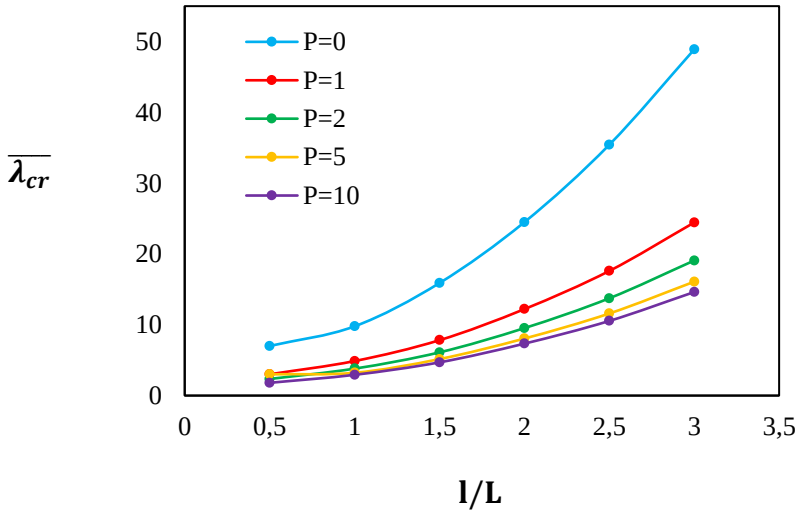

Fig.7 Nondimensionalized critical load factor($\overline{\lambda_{cr}}$) of square plates versus aspect ratio (l/L) with various power index p of the FGM under biaxial compression.

5 CONCLUSION

A four-node finite element based on a higher-order shear deformation theory with five degrees of freedom per node is developed to analyze buckling of functionally graded plates under mechanical loads. The model employs a neutral surface concept to eliminate membrane-bending coupling and uses assumed strain functions satisfying compatibility and rigid body modes. Stiffness, and geometric matrices are derived via the principle of Hamilton. Validation studies confirm accuracy and convergence. The effects of thickness ratio, gradient index, aspect ratio, and loading type are investigated. Results show that critical buckling load decreases with increasing gradient index but increases with thickness and aspect ratios. Uniaxial compression yields higher buckling loads than biaxial compression. The method is promising and will be extended to thermo-mechanical and shell analyses.

REFERENCES

[1] J. N. Reddy, Mechanics of Laminated Composite Plates and Shells: Theory and Analysis, CRC Press, 2004.

[2] M. Koizumi, "The concept of FGM," Ceramic Transactions, vol. 34, pp. 3–10, 1993.

[3] S. Suresh and A. Mortensen, Fundamentals of Functionally Graded Materials, IOM Communications, 1998.

[4] J. R. Cho and I. S. Kim, "Mechanical behavior of functionally graded plates under transverse loading," Composite Structures, vol. 47, no. 1–4, pp. 123–128, 1999

[5] S. A. Sobhani Aragh, M. Z. Kabir, "Thermoelastic analysis of functionally graded plates using finite element method based on higher-order shear deformation theory," Finite Elements in Analysis and Design, vol. 47, no. 6, pp. 751–762, 2011.

[6] J. N. Reddy, "A simple higher-order theory for laminated composite plates," Journal of Applied Mechanics, vol. 51, no. 4, pp. 745–752, 1984.

[7] E. Carrera, "Theories and finite elements for multilayered plates and shells: a unified compact formulation with numerical assessment and benchmarking," Archives of Computational Methods in Engineering, vol. 10, no. 3, pp. 215–296, 2003.

[8] A. Zenkour, "Generalized shear deformation theory for bending analysis of functionally graded plates," Applied Mathematical Modelling, vol. 30, pp. 67–84, 2006.

[9] A. Tati, "A five unknowns high order shear deformation finite element model for functionally graded plates bending behavior analysis," Journal of the Brazilian Society of Mechanical Sciences and Engineering, vol. 43, 2021.

[10] A. B. Sabir and A. Sfendji, "Triangular and rectangular plane elasticity finite elements," Thin-Walled Structures, vol. 21, pp. 225–232, 1995.

[11] L. Belounar and M. Guenfoud, "A new rectangular finite element based on the strain approach for plate bending," Thin-Walled Structures, vol. 43, pp. 47–63, 20

[12] T.Assas, M.Bourezane, and M.Chenafi, "Static, free vibration, and buckling analysis of functionally graded plates using the strain-based finite element formulation". Arch Appl Mech Vol. 94, pp. 2243–2267 (2024). https://doi.org/10.1007/s00419-024-02635-0

[13] A.Tati, "Finite element analysis of thermal and mechanical buckling behavior of functionally graded plates". Arch Appl Mech, vol. 91,, pp. 4571–4587 (2021). https://doi.org/10.1007/s00419-021-02025-w

[14] A.Belounar, F. Boussem, and A. Tati, "A Novel C0 Strain-Based Finite Element for Free Vibration and Buckling Analyses of Functionally Graded Plates." J. Vib. Eng. Technol. Vol.11, pp.281–300 (2023). https://doi.org/10.1007/s42417-022-00577-x

[15] T.Assas, M.Bourezane, and M.Chenafi, "Static, free vibration, and buckling analysis of functionally graded plates using strain approach and Reissner–Mindlin elements". J Braz. Soc. Mech. Sci. Eng.Vol. 47, 498 (2025). https://doi.org/10.1007/s40430-025-05812-6

[16] A.Sadgui , and A.Tati, (2021). "A novel trigonometric shear deformation theory for the buckling and free vibration analysis of functionally graded plates". Mech. Adv. Mater. Struct. Vol.29 pp.6648-6663 (2021),

[17] B.S Reddy, J.S Kumar, C.E Reddy, K.V. K Reddy, "buckling analysis of functionally graded material plates using higher order shear deformation theory". J. Compos. **2013**, 1–12 (2013). https://doi.org/ 10.1155/2013/808764

[18] H.T Thai, Choi, D. H.: An efficient and simple refined theory for buckling analysis of functionally graded plates. Appl. Math. Model. **36**(3), 1008-1022 (2012). https://doi.org/10.1016/j.apm.2011.07.062

[19] Zenkour, A.M., Aljadani, M.H.: Mechanical buckling of functionally graded plates using a refined higher-order shear and normal deformation plate theory. Adv. Aircr. Spacecr. Sci. **5**(6), 615–632 (2018). https://doi.org/ 10.12989/aas.2018.5.6.615